Computational Materials Science 122 (2016) 240–248

Contents lists available at ScienceDirect

Computational Materials Science

journal homepage: www.elsevier.com/locate/commatsci

Mechanical properties study for new hypothetical crystalline phases of ReB_2: A computational approach using density functional theory

Marco Marín-Suárez *, Mario E. Vélez, Jorge David, Mauricio Arroyave-Franco

Departamento de Ciencias Físicas, Escuela de Ciencias, Universidad EAFIT, A.A. 1226, Medellín, Colombia

ARTICLE INFO

Article history:
Received 18 January 2016
Received in revised form 23 May 2016
Accepted 24 May 2016
Available online 6 June 2016

Keywords:
Density functional theory
Rhenium diboride
Elasticity
Super-hard material
Hardness

ABSTRACT

Rhenium diboride (ReB_2) in its $P6_3/mmc$ crystalline structure, is widely known as a super-hard material, and has been studied many times using the Density Functional Theory (DFT) approach. In this work the same chemical composition was studied in three additional unreported hypothetical crystallographic phases by means of DFT with the hybrid functional approach, and the elastic constants of each phase were calculated. The elastic behavior of ReB_2 was analyzed by means of elastic moduli calculations. Additionally, the velocities of the elastic waves of each phase were calculated, along with the Debye's temperatures, also elastic anisotropy is studied. Semi-empirical and empirical models of hardness were used to estimate qualitatively which phases are or are not hard. It has been determined that the elastic moduli of two out of the three hypothetical phases are desirable and the elastic waves move very slow (< 2 km/s) in one of them. These results and the analysis of the bond critical points (bcp) of each phase allow us to conclude that one of them is soft while the other two are hard. The synthesized phase of ReB_2P6_3/mmc was studied in order to compare and confirm the results.

1. Introduction

Theoretical and computational design of new materials with specific properties has covered importance in the search for new applications [1,2], given that this design allows the absence of experimental tests. The process of this design has been applied to rhenium diboride (ReB_2) by means of *ab initio* methods [3,4]. It has been determined that this material in its hexagonal phase $P6_3/mmc$ is super-hard [5], and additional computational and experimental studies have corroborated that assertion [6,7]. This material has been successfully synthesized by means of mixing Re and B powders, and by arc melting [7]. Chung et al. have measured the hardness of hexagonal ReB_2 to be 48.0 GPa at a load of 0.49 N [8], while Levine et al. have measured a hardness of 40.5 GPa at low loads (< 1 N) [9]. Latini et al. have reported a value of 49.9 at a load of 0.49 N [10], confirming the super-hard nature of ReB_2.

In addition, computational studies have determined the electronic composition of this material. Based on this and semiempirical models [11,12] such those of Gao [13,14] and Šimůnek [15], they are able to obtain the intrinsic hardness of this solid. Other mechanical properties such as the elastic moduli have been calculated by DFT (Density Functional Theory) [16–19] and these results allow better analysis of the hardness through many existent correlations [5].

Other researches [20–22] have analyzed the mechanical and electronic properties of different hypothetical phases of the same material by means of *ab initio* methods. Hao et al. has made these studies on the *Pmmn* symmetry of ReB_2 [20]. This material has been determined to be little compressible, and its electronic structure has lead to believe it could be a hard material on the same level as ReB_2 in the $P6_3/mmc$ phase. The mechanical properties are also similar to those of the $P6_3/mmc$ rhenium diboride. Zhong et al. studied other ReB_2 phases such as the $R\bar{3}m$ giving rise to a hypothetical material with properties similar to those of the synthesized phase [22]. Also Mazdziarz et al. have studied thermodynamical, optical and phonon properties of different hypothetical phases of ReB_2 [23].

Based on these studies and results one can suppose that there could be other phases of ReB_2 with similar mechanical properties. These new phases could have a similar hard behavior, because the electronic structure would be similar. New hypothetical phases of ReB_2 can be analyzed by means of DFT methods, avoiding a direct experimental study of the material. We focus on three phases of ReB_2, orthorhombic, hexagonal and face centered cubic. The calculations on this crystals include elastic constants, elastic moduli, elastic anisotropy factors, velocity of elastic wave and Debye's

* Corresponding author.
E-mail address: mmarins@eafit.edu.co (M. Marín-Suárez).

http://dx.doi.org/10.1016/j.commatsci.2016.05.032
0927-0256/

temperature. Besides calculations of cohesive energy, energy of formation. The calculations of bond critical points (bcp) along with the quantities previously determined allow to compare the hardness of these three phases with that of the $P6_3/mmc$ structure. These calculations are performed for the reported $P6_3/mmc$ structure in order to validate the process.

This document is organized as follows. First, there is an introduction that presents the research and its objectives. Second are the methods, including a description of the computational processes as well as the crystalline structures used in this study. Then the results are presented along with a discussion of them, and finally some conclusions extracted from those results are presented.

2. Methods

2.1. Computational details

First-principle calculations were performed with DFT, as implemented in the software CRYSTAL09 [24]. The exchange and correlation interactions were described using the PBE0 [25] hybrid functional which mixes the general gradient approximation (GGA) [26,27] PBE [28,29] functional and Hartree–Fock exchange interaction. A Pack–Monkhorst [30] mesh of $10 \times 10 \times 10$ in the first Brillouin zone was used for the discretization of the reciprocal space.

The wave functions of boron and rhenium have been approximated by the basis sets of gaussian functions POB_TZVP [31] and Re_cora_1991, respectively. Gaussian functions were used since they have been successfully applied to all-electron calculation as elastic constants calculations [24,32–34]. These particular sets of functions were chosen given that they reproduce faithfully the crystal structure of the experimental ReB_2 in phase $P6_3/mmc$ (see Table 1).

For the geometry optimizations the tolerances were set to be 0.015 eV/Å for the rms value of the energy gradient, 6.350×10^{-4} Å for the rms value of the displacement, and 2.721×10^{-6} eV for the difference in total energy. The elastic constant calculations were made using the CRYSTAL09 code [33,32]. For these process three default deformations with a step of 0.01 were performed in order to calculate the second derivative of the energy with respect to strains. For this calculations the tolerances were the same as for optimization.

The wave's velocities were determined using two approaches: anisotropic and isotropic. For the anisotropic calculations the software GNU Octave [35] was used along with the package of functions MSAT (MATLAB Seismic Anisotropy Toolbox) [36]. The toolbox calculates these quantities based on Christoffel's formula

$$AU = UV^2.$$

Where A is the matrix with entries $A_{kl} = c_{ijkl}q_jq_i/\varrho$, where c_{ijkl} is the fourth-rank tensor of elastic constants, ϱ is the density of the solid, and q_i is the i-th component of the unitary vector in the propagation direction. Diagonalizing this matrix one obtains the diagonal matrix V^2 which contains the squared velocities of each one of the three modes.

The determination of the bond critical points was made by means of the topological analysis program TOPOND [37]. This search was made in the asymmetric unit of the crystal through an eigenvector-following algorithm which runs during ten steps with eight neighbors for each point in a radius of 10 Å. These processes were performed within a box defined in the intervals $[0;1]\times[0;1]\times[0;1]$ with a discretization of 0.025 in each direction. No further constraints were applied. To improve the calculations these were focused on the bond critical point.

2.2. Studied phases

This study was performed on three hypothetical crystalline phases of ReB_2 and the widely known $P6_3/mmc$ structure. The crystallographic properties of each phase are shown in Table 1. In this table the atomic package factor (APF) has been calculated with regard to the covalent radii of the atoms for the crystals 1–3 and the ionic radius for the crystal 4. In order to determine stability the cohesive energy (E_{coh}) was calculated from the formula [38,23]

$$E_{coh} = \frac{E_{Tot}^{ReB_2} - nE_{Tot}^{Re} - mE_{Tot}^{B}}{n+m}. \quad (1)$$

where $E_{Tot}^{ReB_2}$, E_{Tot}^{Re} and E_{Tot}^{B} are total energies of ReB_2, Re single atom and B single atom, respectively; m and n are the number of Re and B atoms in unit cell, respectively. This quantity is the energy needed to dissociate the unit cell of each phase.

Also the formation energy (ΔH) was calculated based on the chemical equation $\frac{1}{2}Re_2 + \frac{1}{6}B_{12} \rightarrow ReB_2$, and on the expression [39]

$$\Delta H = E_{coh}^{ReB_2} - \frac{1}{2}E_{coh}^{Re} - \frac{1}{6}E_{coh}^{B}, \quad (2)$$

with E_{coh}^{Re} and E_{coh}^{B} being the cohesive energies of the most stable crystalline phases of rhenium and boron, respectively. For the boron the α-B structure in phase $R\bar{3}m$ was used and for rhenium the hexagonal $P6_3/mmc$ structure. Formation enthalpy is the energy needed so that the reaction takes place. In order to use Eq. (1), the structures of boron and rhenium were optimized with the same convergence criteria than the ReB_2 phases and with the same basis set for each atom. The results for E_{coh} and ΔH are in Table 1 both given in eV/atom.

The Wyckoff positions, symmetry and points of each atom in every single structure are shown in Table 2. These data have been obtained from the Bilbao Crystallographic Server [40].

Table 1
Space group (SG), lattice parameters a, b and c (in Å), atomic packing factor (APF), density ϱ (in kg/m^3), cohesive energy E_{coh} (in eV/atom) and formation enthalpy (in eV/atom) of each crystalline phase of ReB_2.

Crystal	SG	a	b	c	APF	ϱ	E_{coh}	ΔH
1	$Immm$	4.947	2.898	3.970	0.680	12195.79	−10.43	−2.58
2	$P\bar{6}m2$	3.321	3.321	3.219	0.630	11260.79	−10.70	−2.85
3	$P6_3/mmc$	2.837	2.837	7.392	0.752	13466.00	−11.65	−3.80
3[a]	$P6_3/mmc$	2.900	2.900	7.478	–	–	–	–
3[b]	$P6_3/mmc$	2.897	2.897	7.472	–	–	–	–
3[c]	$P6_3/mmc$	2.903	2.903	7.485	–	–	–	–
4	$Fm3m$	4.917	4.917	4.917	0.652	11577.05	−10.25	−2.40

[a] Synthesized structure by [8].
[b] Synthesized structure by [9].
[c] Synthesized structure by [10].

Table 2
Wyckoff position, symmetries and points of the Re and B atoms.

Crystal	Re			B		
	Wyckoff position	Symmetry	Point	Wyckoff position	Symmetry	Point
1	2c	$mmm(D_{2h})$	$(0,0,\frac{1}{2})$	4e	$mm2(C_{2v})$	$(-\frac{7}{40},0,0)$
2	1a	$\bar{6}m2(D_{3h})$	$(0,0,0)$	2i	$3m(C_{3v})$	$(-\frac{1}{3},\frac{1}{3},\frac{1}{4})$
3	2c	$\bar{6}m2(D_{3h})$	$(\frac{1}{3},-\frac{1}{3},\frac{1}{4})$	4f	$3m(C_{3v})$	$(\frac{1}{3},-\frac{1}{3},-\frac{1}{2})$
4	4b	$m\bar{3}m(O_h)$	$(-\frac{1}{2},\frac{1}{2},\frac{1}{2})$	8c	$\bar{4}3m(T_d)$	$(\frac{1}{4},-\frac{1}{4},-\frac{1}{4})$

In crystal 1 there are six atoms (two of Re and four of B) per conventional cell. The atoms of rhenium are coordinated by four boron atoms arranged in a rectangle to give a D_{2h} symmetry. Atoms of boron in this structure are surrounded by two rhenium atoms as first-nearest neighbors forming a triangle with C_{2v} symmetry.

The crystal 2 has nine atoms (three of Re and six of B) in the conventional cell. In this structure rhenium is coordinated by six boron atoms forming a triangular prism with the Re atom at its center giving a D_{3h} symmetry. The boron atoms are surrounded by three rhenium atoms, forming a pyramid where the boron is at the top. This shape gives arise to a C_{3v} symmetry.

The crystal 3 possesses eighteen atoms in the conventional cell (six of Re and twelve of B). Although the Wyckoff positions of atoms in the crystal 3 are different from those of the crystal 2 they share the coordination numbers and the symmetry point group.

In crystal 4 there are twelve atoms per conventional cell (four of Re and eight of B). The rhenium atoms are in cubic sites coordinated by eight boron to give an O_h symmetry, while the boron atoms are in tetrahedral sites surrounded by four rhenium atoms, forming a T_d symmetry. The conventional cells of each crystalline structure are shown in Fig. 1.

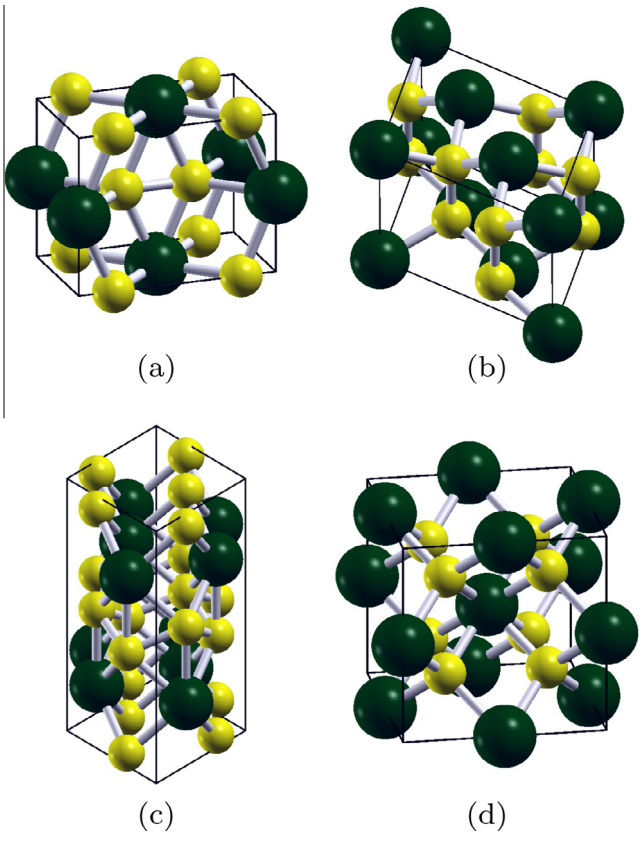

Fig. 1. Conventional cells of (a) crystal 1, (b) crystal 2, (c) crystal 3, and (d) crystal 4. The big spheres represent Re atoms, the little ones B atoms. Images obtained with XCrySDen [41].

3. Results and discussion

3.1. Elastic constants

The elastic stiffness tensor c_{ijkl} relates the stress (σ_{ij}) and the strain (ϵ_{ij}) tensors in a solid through the Hooke's law

$$\sigma_{ij} = c_{ijkl}\epsilon_{kl},$$

conversely

$$\epsilon_{ij} = s_{ijkl}\sigma_{kl}.$$

The s_{ijkl} tensor is called the elastic compliance tensor and is the inverse of c_{ijkl}. The elastic stiffness tensor is a fourth-rank tensor so it has 81 elements. For symmetry reasons this number of elements is converted to a symmetric 6×6 matrix. There are only 21 independent terms and the elastic constants c_{ijkl} are written as c_{ij}. These quantities are related by the Voigt notation [42]. Table 3 presents the results for the elastic constants in GPa for each studied crystal.

Results in Table 3 for crystal 1 show that it has a low compressibility along c and b axis due to the values of c_{33} and c_{22} respectively. It also has an unusually high value for c_{55} which means that there is a high resistance to distortion when applying an stress on $\{001\}$ planes in (100) direction. On the opposite there is an extremely small value for c_{66} meaning there is almost no resistance to stresses on $\{010\}$ planes in (100) direction.

Crystal 2 is very resistant to compression along c axis unlike the other two axes given the high value of c_{33} respect to c_{11}. Remarkably this structure has a similar response to shear stresses than crystal 1, it has large resistance to stresses on $\{001\}$ planes in $(1\bar{1}0)$ and (110) directions due to the high value of c_{44}. But presents barely resistance on $\{1\bar{1}0\}$ planes in (110) direction given the low constant c_{66}.

Crystal 3 has the highest constants for compressibility, the unusually high constant c_{33} means a low compressibility along c axis, added to the high value of c_{11} gives arise to an ultra-incompressible material [43]. The values for the shear constants c_{44} and c_{66} are consequence of an uniform behavior of crystal 3, unlike crystals 1 and 2, to shear stresses with medium values for elastic resistance.

Crystal 4 has the highest values for constant c_{12} which means that this structure has a considerable resistance to the Poisson effect which sums to the incompressibility. On the contrary c_{11} constant is low compared to those corresponding to other crystals which does not contributes to a high resistance to compression. The constant c_{44} is low meaning a minimum rigidity when crystal 4 is submitted to shear stresses.

Results for crystal 3 in Table 3 were compared with theoretical results from references [3,17,18]. The differences are less than 8% for c_{11}, c_{13}, c_{33} and c_{44} but are larger for the quantity c_{12}. This can be understood under the consideration that just one strain is not enough to calculate this number and it depends on the calculations of other constants. Thus the large difference in the determination of c_{12} is due to the propagation of other errors [44].

Table 3
Elastic constants in GPa for all the structures.

Crystal	c_{11}	c_{12}	c_{13}	c_{22}	c_{23}	c_{33}	c_{44}	c_{55}	c_{66}
1	570.61	285.34	266.45	452.09	156.63	623.14	217.17	989.20	9.52
2	382.19	340.68	94.64	382.19	94.64	768.51	704.54	704.54	20.75
3	697.96	205.39	137.01	697.96	137.01	1122.20	287.98	287.98	246.29
4	320.45	304.40	304.40	320.45	304.40	320.45	62.92	62.92	62.92

Also results for crystal 3 were compared with the experimental ones from [45] giving errors less than 10% for c_{11}, c_{12}, c_{33} and c_{44}, and 25% for c_{13}. This comparison allows to confirm that the election of the basis sets referred in subSection 2.1 was good.

The values in Table 3 satisfy the generalized elastic stability criteria given in [22]. For cubic crystals the conditions are $c_{11} > 0$, $c_{44} > 0$, $c_{11} - c_{12} > 0$, $c_{11} + 2c_{12} > 0$; for hexagonal phases $c_{44} > 0$, $c_{11} - c_{12} > 0$, $[c_{33}(c_{11} + c_{12}) - 2c_{13}^2] > 0$; and for orthorhombic crystals are $c_{ii} > 0$, $[c_{11} + c_{22} + c_{33} + 2(c_{12} + c_{13} + c_{23})] > 0$, $c_{11} + c_{22} - 2c_{12} > 0$, $c_{11} + c_{33} - 2c_{13} > 0$, $c_{22} + c_{33} - 2c_{23} > 0$. Regarding thermodynamic stability is easy to see from Table 1 that all four structures are stable since formation enthalpy is negative. Crystal 3 is the most stable followed by crystal 2, crystal 1 and finally the less stable is crystal 4.

3.2. Calculation of directional elastic moduli

Directional or anisotropic elastic moduli were calculated following the formulas given in [46]. These expressions are reached by considering only stress in the directions $\hat{\mathbf{m}}$ and $\hat{\mathbf{n}}$ and the strain that one wants to analyze, in addition to Hooke's law.

For the Young's modulus there is need of only one direction $\hat{\mathbf{n}}$, given that this modulus measures the resistance to pure tension stresses. This modulus is expressed as [46]

$$E(\hat{\mathbf{n}}) = \frac{1}{n_i n_j s_{ijkl} n_k n_l}.$$

The n_i's are the direction cosines in the direction of $\hat{\mathbf{n}}$. For each structure the last expression is expanded and a equation is obtained. These equations can be visualized by plotting a quadric surface in which the distance between the origin and the surface is equal to the Young's modulus in that direction, so the more spheric the surface the more isotropic is the Young's modulus. These surfaces are shown in Fig. 2 for each crystal, the origin of the coordinate system is in the center of each figure.

In order to give some hints about the anisotropy in planes the shear anisotropy factors are calculated. The anisotropy factors [47] on planes {100}, {010} and {001} are, respectively

$$A_1 = \frac{4c_{44}}{c_{11} + c_{33} - 2c_{12}}, \quad A_2 = \frac{4c_{55}}{c_{22} + c_{33} - 2c_{23}},$$
$$A_3 = \frac{4c_{66}}{c_{11} + c_{22} - 2c_{12}},$$

these factors are unity for an isotropic material on the referred planes. The more it deviates from one the more anisotropy there are on the plane. The factors for each structure are in Table 4.

Observing Table 4 one can infer that crystal 1 is the most anisotropic since all its factors deviate from 1 and all of them are different. The value of each factor and differences between factors are reflected into Fig. 2 projecting plots on *xy*, *yz* and *xz* planes. It can be seen from Fig. 2a that each projection is different in its form which is in accordance to all anisotropy factor of crystal 1 being different. Since all factors of crystal 1 differ from one therefore none of those projections is a circumference. The anisotropy factor equal to unity for crystals 2 and 3 reflect that they are hexagonal phases, Fig. 2b and c support that fact. Table 4 shows that every anisotropy factor for crystal 4 are different than unity which confirms the fact that projections of Fig. 2d are not circumferences. Since crystal 4 is cubic all its anisotropy factors are equal.

Fig. 2a reveals that crystal 1 has its peak of resistance to tension in direction (101) and equivalents since c_{33} and c_{55} dominate the Young's modulus in this direction and those constants are very large for this structure. The small value of c_{66} makes this modulus narrow in the *xy* plane. For crystal 2 the maximum Young's modulus is in all directions that have a polar angle of $\pm\pi/4$ rad given the high values of c_{33}, c_{44} and c_{55}, as in crystal 1 the low value of c_{66} produces a narrow waist in the plot of Fig. 2b. Crystal 3 has its maximum value of the modulus along the *z* axis the reason is that enormous value of c_{33} in Table 3. Crystal 4 has the largest Young's modulus along (111) direction and equivalent since it is a cubic lattice and $c_{33} < c_{12} + \frac{1}{2}c_{44}$.

3.3. Calculation of elastic moduli for polycrystalline aggregates

Non-directional or isotropic bulk and shear moduli of the four crystals were calculated using the Voigt approximation [42], which is an upper limit, and the Reuss approximation [48], which is a lower limit. Additionally the Voigt–Reuss–Hill approximation [49] was used to calculate the elastic moduli.

The Voigt approximation is given by the two equations

$$B_V = \frac{1}{9}(c_{11} + c_{22} + c_{33}) + \frac{2}{9}(c_{12} + c_{13} + c_{23}), \tag{3}$$
$$G_V = \frac{c_{11} + c_{22} + c_{33} - (c_{12} + c_{13} + c_{23}) + 3(c_{44} + c_{55} + c_{66})}{15}. \tag{4}$$

The Reuss approximation is expressed as follows

$$B_R = \frac{1}{s_{11} + s_{22} + s_{33} + 2(s_{12} + s_{13} + s_{23})}, \tag{5}$$
$$G_R = \frac{15}{4(s_{11} + s_{22} + s_{33}) - 4(s_{12} + s_{13} + s_{23}) + 3(s_{44} + s_{55} + s_{66})}. \tag{6}$$

As said before these two approximations constitute upper and lower bounds for the real bulk and shear moduli of a crystalline aggregate, so an obvious approximation would be an average between these two quantities. This is the known Voigt–Reuss–Hill approximation, which can be written as

$$B = \frac{B_V + B_R}{2}, \tag{7}$$
$$G = \frac{G_V + C_R}{2}. \tag{8}$$

Young's modulus and Poisson's ratio for crystalline aggregates can be expressed as [49]

$$\nu = \frac{1}{2}\left[1 - \frac{3G}{3B + G}\right], \tag{9}$$
$$\frac{1}{E} = \frac{1}{3G} + \frac{1}{9B}. \tag{10}$$

A measure of the anisotropy in polycrystalline aggregates is the "universal" anisotropy factor $A^U = 5G_V/G_R + B_V/B_R - 6$, which is

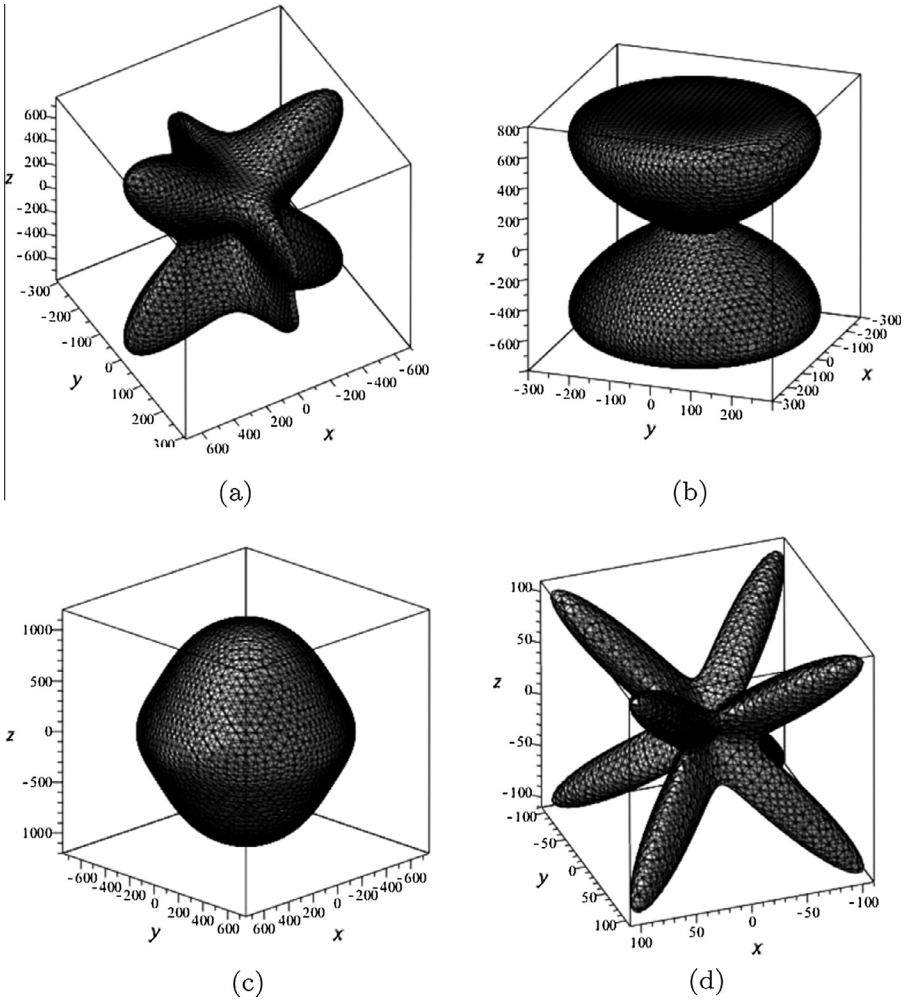

Fig. 2. Surface representation of directional Young modulus for (a) crystal 1, (b) crystal 2, (c) crystal 3 and (d) crystal 4.

Table 4
Anisotropy factors A_1, A_2 and A_3 for each studied phase of ReB_2.

Crystal	1	2	3	4
A_1	1.31	2.93	0.74	7.84
A_2	5.19	2.93	0.74	7.84
A_3	0.08	1.00	1.00	7.84

zero for an isotropic bulk. Using the Eqs. (3)–(10) the elastic moduli of a crystalline aggregate composed of all four phases of ReB_2 are calculated. These data and A^U are given in Table 5; Young's, bulk and shear moduli are given in GPa.

The results for crystal 3 have been compared to those in references [3,17,18], and all the differences are under 15%, indicates that the present study is going in the right direction. From Table 5 it is possible to determine that there are three little compressible phases, but crystal 4 has a very low shear modulus, which could mean that this material is not hard at all according to some correlations [5]. Its low Poisson's ratio supports this assertion. Crystals 1 and 2 have almost equal shear moduli, although the first is less compressible than the last. It is possible that those two phases have a very similar hardness. Furthermore their Young's modulus and Poisson's ratio are very alike so these two solids are mechanically similar in a macroscopic way, but no microscopically (see Table 3). It is easy to conclude that the highest elastic properties come from crystal 3 being highly incompressible and very rigid. When combining those properties in diborides the result is often a super-hard material [5] as expected. Regarding A^U it can be seen that for crystal 3 it is the closest to zero thus is the most isotropic of all phases as expected for an hexagonal crystal [50]. Crystal 1 is the most anisotropic since it is orthorhombic and all c_{ij}'s are different, hence all anisotropy factors are different.

3.4. Calculation of velocities of the anisotropic elastic waves

The calculation of the velocities of the anisotropic waves was performed with respect to the seven directions shown in the first row of Table 6. In order to perform these calculations it was necessary to determine the density of each phase. This quantity is already known from Table 1.

The velocities of the longitudinal (v_l) and the two transverse (v_{t1} and v_{t2}) modes in each direction for each crystal are shown in Table 6 in km/s.

The peak value of Young's modulus in crystal 1 along (101) is the reason for the high value of v_l in the same direction (see Table 6). Also the large value of v_{t1} in (001) is due to the high constant c_{55} additionally the small v_{t2} along (100) and (010) is explained by the small c_{66}. Crystal 2 has a high value for longitudinal velocities in (101) and (011) due to the Young's modulus has its largest values on those directions. The large value for v_{t1} along (001) and the small one for v_{t2} in (100) are consequence of large c_{44} and small c_{66} respectively. For crystal 3 it is consistent that v_l is maximum in (001) with the peak of Young's modulus in this

Table 5
Elastic moduli of the crystalline aggregate composed of the three phases of ReB_2. The Young's, bulk and shear moduli are given in GPa.

Crystal	B_V	B_R	G_V	G_R	B	G	E	ν	A^U
1	340.30	327.55	305.67	39.99	333.92	172.83	442.17	0.27	33.25
2	288.09	286.29	345.62	48.57	286.92	197.09	379.99	0.28	30.58
3	386.32	375.23	300.36	286.54	380.77	293.45	700.42	0.19	0.27
4	314.40	314.40	39.74	11.09	314.40	25.41	74.23	0.46	12.91

direction as seen in Fig. 2c. Crystal 4 has a maximum for v_l along (1 1 1) as can be seen from Table 6 due to the peak value of Young's modulus in that direction (see Fig. 2d). Also the low values of all shear wave's velocities are explained by the small values of c_{44}, c_{55} and c_{66}.

3.5. Calculation of velocities of elastic waves for polycrystalline aggregate

In the same way that elastic moduli were calculated as a single number, it is possible to determine the velocities of the elastic waves as a number not as a function of direction. The calculations are carried out for a polycrystalline aggregate composed of the respective phase. Because of this the elastic moduli in these calculations are Voigt–Reuss–Hill approximations. The elastic longitudinal wave's velocities are given by

$$v_l = \sqrt{\frac{3B + 4G}{3\varrho}}. \tag{11}$$

For the two polarizations of shear wave's velocities the expression is

$$v_t = \sqrt{\frac{G}{\varrho}}. \tag{12}$$

Also there is an average for those velocities that is helpful for comparison

$$v_m = \left[\frac{1}{3}\left(\frac{2}{v_t^3} + \frac{1}{v_l^3}\right)\right]^{-1/3}. \tag{13}$$

After obtaining these averages, the Debye temperature of each phase can be calculated according to the relation [44]

$$\theta_D = \frac{h}{k_B}\left[\frac{3n}{4\pi}\left(\frac{\varrho N_A}{M}\right)\right]^{1/3} v_m. \tag{14}$$

Where n is the number of atoms per chemical formula, M is the molar mass, h is Planck's constant, k_B is Boltzmann's constant and N_A is Avogadro's number.

Table 7
Elastic wave's velocities for polycrystalline aggregate in km/s, and Debye's temperature in K.

Crystal	v_l	v_t	v_m	θ_D
1	7.305	3.764	4.215	593.87
2	6.987	4.184	4.630	635.23
3	7.571	4.668	5.150	749.98
3[a]	–	–	–	716.00
3[b]	–	–	–	782.00
3[c]	–	–	–	774.00
3[d]	–	–	–	749.00
4	5.484	1.481	1.690	234.02

[a] Ref. [3].
[b] Ref. [17].
[c] Ref. [18].
[d] Ref. [51].

Table 7 shows the calculations carried out using Eqs. (11)–(13) in km/s. Also the Debye temperature in K is shown in this table calculated using Eq. (14).

There is a big difference between the average velocity of crystal 4 and the others, which reveals the low rigidity of this phase with respect to the other three. This result is consistent with the low values of c_{11} and c_{44}, that reflects directly in results from Tables 7 and 5. Crystal 3 is the most rigid of the four.

Notably the Debye's temperature found for crystal 3 is in accord with other works. It is remarkably close to the value provided in reference [51]. There is a relation between Debye's temperature (θ_D) of the material and the hardness H [52]

$$\theta_D \propto H^{1/2} V^{1/6} M^{-1/2},$$

where V is the volume of a conventional cell and M is the molar mass of the solid. Thus, one should expect a super-hard material to have a high average wave velocity and hence a high Debye's temperature, as actually occurs with crystal 3. The other crystals 1 and 2 have good rigidity, but not as good as crystal 3, as expected from Table 4, so we anticipate that these phases are not as hard as crystal 3.

Table 6
Phase velocities of elastic waves for all crystals in km/s.

Crystal	Direction	(100)	(010)	(001)	(110)	(101)	(011)	(111)
1	v_l	9.006	6.088	9.006	7.032	10.790	6.831	9.140
	v_{t1}	6.840	4.219	7.148	5.803	3.679	6.398	4.015
	v_{t2}	0.883	0.883	4.219	3.004	3.048	3.901	3.431
2	v_l	7.910	7.910	8.261	7.910	9.661	9.661	9.435
	v_{t1}	5.825	5.852	7.910	5.825	5.675	5.675	4.699
	v_{t2}	1.357	1.357	7.910	1.357	4.508	4.508	4.348
3	v_l	7.103	7.103	9.075	7.103	7.845	7.845	7.489
	v_{t1}	4.622	4.622	4.622	4.622	5.121	5.121	5.134
	v_{t2}	4.126	4.126	4.622	4.126	4.381	4.381	4.298
4	v_l	5.261	5.261	5.261	5.693	5.693	5.693	5.831
	v_{t1}	2.331	2.331	2.331	2.331	2.331	2.331	1.507
	v_{t2}	2.331	2.331	2.331	0.832	0.832	0.832	1.507

Table 8
Properties of bond critical points. Density of electrons ρ given in 10^{-7} pm^{-3}, Laplacian of density $\nabla^2\rho$ given in 10^{-10} pm^{-5}, and eigenvalues of the Hessian of ρ given in 10^{-10} pm^{-5}.

Crystal	Bond	ρ	$\nabla^2\rho$	λ_1	λ_2	λ_3
1	B–B	8.916	−4.658	−3.765	−2.269	1.376
	Re–B	5.944	0.652	−1.593	−0.748	3.017
	Re–B	6.012	−0.603	−1.714	−1.521	2.607
2	Re–B	7.430	−0.893	−2.582	−1.231	2.921
	Re–Re	1.688	0.579	−0.193	−0.193	0.989
	B–B	9.727	−6.155	−3.669	−3.669	1.182
	B–B	9.332	−2.655	−1.810	−1.810	0.941
3	B–B	7.295	−2.824	−2.848	−1.231	−1.255
	Re–B	6.079	−0.386	−1.882	−1.231	2.703
	Re–B	5.606	1.810	−0.652	−0.652	3.114
4	Re–B	9.659	8.593	−1.641	−1.641	2.486

3.6. Determination of bond critical points

The bond critical points of each one of the phases are determined and from this data it is possible to describe the types of bonds that are present in each crystal. This information provides a better mechanical description of each material. Table 8 shows some properties of the bond critical points like the Laplacian and eigenvalues of the Hessian matrix. All those properties are given in SI units.

Table 8 gives arise to some interesting observations when analyzed with The Quantum Theory of Atoms in Molecules (QTAIM) [53]. However this theory is not a unique recipe to classify chemical bonds [54] but gives some interesting hints regarding bonding structure.

Crystal 1 has B–B and Re–B bonds with a negative Laplacian, indicating that those two bonds are covalent [53]. The large difference between λ_1 and λ_2 in the first bond means that this is a highly localized bond, unlike the second one [53]. The other Re–B bond is evidently ionic and localized as indicated by its positive Laplacian and the large difference between λ_1 and λ_2. This bond has a high projection along the c axis of the crystal its localization added to its high concentration per volume give arise to a high elastic constant c_{33}. The high value of c_{55} is also explained by this Re–B ionic bond given its high projection perpendicular to a–c plane. On the opposite, the low value of c_{66} is due to that resistance to a *xy* stress is exerted mostly by the covalent unlocalized Re–B bond.

Crystal 2 has three covalent bonds, one Re–B and two physically different B–B. The first bond is highly localized but the two bonds between borons are completely unlocalized given the equality between λ_1 and λ_2. Besides, this phase has one ionic bond Re–Re that is completely unlocalized which could possibly mean that in this phase a metallic bond exists. Given that the majority of those bonds are directed or have a high projection along c axis the constant c_{33} is higher than c_{11} meaning a low resistance along other axes. As a consequence of this low resistance along axes perpendicular to c axis the constant c_{66} is very low.

In crystal 3 there is one covalent localized B–B bond and a Re–B which is covalent and highly localized, as well as an ionic Re–B bond that is completely unlocalized. Adding the covalency, high localization and the direction along c axis of bond B–B one would expect a high value of c_{33}. If the projection along c axis of a covalent and highly localized bond is added to the previous one then one should expect not a high value of c_{33} but an outstandingly high value as actually happens in crystal 3. Finally, crystal 4 only has one type of bond which is a completely unlocalized ionic Re–B bond. The high concentration of this type of bonds and given that it has projections along all axes makes this structure little compressible. But the ionic and unlocalized bonds give arise to low shear resistance.

3.7. Qualitative hardness analysis

In this section the hardness of each phase is predicted in a qualitative and comparative way. Recall that there are some correlations [5] between shear modulus and hardness or elastic wave's velocities and hardness. There are also some models such as Gao's [13] and Šimůnek's [15] which assert that the covalent and highly localized bonds allow the formation of hard phases. All the results obtained previously help this analysis.

Crystal 4 has a very low rigidity (see Table 5) and the elastic waves are very slow (see Tables 6 and 7). Additional, only completely unlocalized ionic bonds exist in this material. Taking this into account one can conclude that this material is in fact a soft material in spite of its incompressibility. The opposite conclusion is reached when looking into the properties of the known superhard material ReB_2 in its $P6_3/mmc$ phase (crystal 3). This solid has a very large shear modulus and is highly little compressible. Also, the elastic waves move very fast in this material, suggesting that this is a hard material. Additionally, having those highly localized covalent Re–B and B–B bonds makes this material a hard one in spite of the unlocalized ionic Re–B bond.

Crystal 2 shows a large shear modulus (see Table 5) and propagates relatively fast elastic waves (see Table 7) but not as fast as crystal 3. The presence of the metallic Re–Re bond reduces the hardness of the solid [55]. Also, the covalent B–B bonds are completely unlocalized. Luckily there is a highly localized covalent Re–B bond. Although these properties give arise to a hard material the hardness of crystal 2 is not even close to that of crystal 3.

In crystal 1 it is easy to see that its elastic moduli are very similar to those of crystal 2, but it propagates much slower elastic waves than crystal 2, leading to the assumption that this material is less hard than crystal 2. Crystal 1 has localized covalent B–B and Re–B bonds, as well as an unlocalized ionic bond, leading to the assumption that crystal 1 has a more favorable structure for hardness than crystal 2. However, this structure has a higher density of covalent B–B bonds than crystal 1 which is an important factor that increases the hardness [14].

Thus, one could conclude that the order in the hardness of the studied materials should be: first crystal 3, then crystal 2, followed by crystal 1 and 4.

4. Conclusions

We have used first principle DFT methods with hybrid functionals (GGA + Hartree–Fock) for study four crystalline phases of ReB_2, three of them are hypothetical, with space group *Immm*, $P\bar{6}m2$ and $Fm\bar{3}m$, and the other has been found experimentally in phase $P6_3/mmc$. The lattice parameters and elastic constants of the reported structure are in good agreement with experimental reports. The computational method that arose these results were applied to the hypothetical phases and allowed an structural description of them. Determination of the cohesive energy and formation energy for each crystal allowed to conclude the thermodynamical stability of all phases and the reported one was the most stable.

Elastic constants for ReB_2 were calculated using DFT and a good agreement (near 10%) between these calculations for phase $P6_3/mmc$ and the experimental measures [45] as well as other theoretical studies [3,17,18] was found. Important is that calculated elastic constants reproduce the ultra-incompressible behavior of experimental ReB_2. This behavior is also observed in the other hypothetical phases from theoretical elastic constants. However for crystals in phases *Immm* and $P\bar{6}m2$ there is a constant giving a poor behavior to shear stresses, and for $Fm\bar{3}m$ phase there is barely resistance to those kind stresses. From those calculated

constants it was possible to determine Young's, shear and bulk modulus as well as Poisson ratio in Voigt's, Reuss's and Hill's approximations. The analysis of the elastic behavior from these moduli is in perfect accordance with the one made with elastic constants. As a consequence of these behaviors the calculated average of elastic wave's velocities is the largest for $P6_3/mmc$ structure and the lowest for $Fm\bar{3}m$, also the Debye's temperatures were calculated and obtained an excellent agreement for the one of the $P6_3/mmc$ phase compared with theoretical studies [3,17,18,51]. The largest Debye's temperature is for $P6_3/mmc$ polymorph and the lowest for the $Fm\bar{3}m$ one.

Elastic constants also allowed to study the elastic anisotropy of all phases, surfaces for directional Young's modulus were plotted helping to determine the directions of maxim for this modulus in each phase. The calculation of shear anisotropy factors allowed to describe these plots and there was an accordance between these descriptions and the actual figures. Through elastic constants and the Christoffel's equation the anisotropic behavior of elastic waves in each solid was analyzed, this discussion was in perfect agreement with shear anisotropy factors and directional elastic moduli. In order to evaluate anisotropy in bulk the universal anisotropy factor was calculated giving a high isotropy for phase $P6_3/mmc$ and a low one for $Immm$ and $P\bar{6}m2$.

Knowing that chemical bonds are responsible for the resistance to distortion, then we decided to perform a bond critical point study with the QTAIM [53] approach for each structure. Determined that all solids have more than one type of localized and unlocalized bonds except for the $Fm\bar{3}m$ which has only ionic unlocalized ones. The type and orientations of bonds allow an analysis of the elastic resistance which is in accordance to that of the elastic constants. Adding the types of bonds present and its localization to the results for elastic behavior we were able to describe qualitatively the hardness of each phase based on correlations [5] and semi empirical microscopic models [13,15]. Concluding that the phase $P6_3/mmc$ is the hardest, the $Immm$ and $P\bar{6}m2$ ones are hard but not at the level of the previous phase, finally the structure $Fm\bar{3}m$ is a soft solid.

Acknowledgements

The authors would like to thank Universidad EAFIT for funding the Project 690-000034 "Propiedades electrónicas y ópticas del ReB_2". As well as the personal of center of computation Apolo for supporting the calculations made in this research.

References

[1] G. Soto, M. Moreno-Armenta, A. Reyes-Serrato, Study on the formation of rhenium borides by density functional calculations, Comput. Mater. Sci. 44 (2008) 628–634, http://dx.doi.org/10.1016/j.commatsci.2008.05.012.
[2] J. Haines, J. Léger, G. Bocquillon, Synthesis and design of superhard materials, Annu. Rev. Mater. Res. 31 (1) (2001) 1–23, http://dx.doi.org/10.1146/annurev.matsci.31.1.1.
[3] X. Hao, Y. Xu, Z. Wu, D. Zhou, X. Liu, X. Cao, J. Meng, Low-compressibility and hard materials ReB_2 and WB_2: prediction from first-principles study, Phys. Rev. B 74 (2006) 224112, http://dx.doi.org/10.1103/PhysRevB.74.224112.
[4] E. Deligoz, K. Colakoglu, Y.O. Ciftci, Lattice dynamical and thermodynamical properties of ReB_2, RuB_2, and OsB_2 compounds in the ReB_2 structure, Chin. Phys. B 21 (10) (2012) 106301, http://dx.doi.org/10.1088/1674-1056/21/10/106301.
[5] A.L. Ivanovskii, Mechanical and electronic properties of diborides of transition 3d–5d metals form first principles: toward search of novel ultra-incompressible and super-hard materials, Prog. Mater. Sci. 57 (09) (2012) 184–228, http://dx.doi.org/10.1016/j.pmatsci.2011.05.004.
[6] J.B. Levine, S.H. Tolbert, R.B. Kaner, Advancements in the search for superhard ultra-incompressible metal borides, Adv. Funct. Mater. 19 (3519–3533) (2009) 76–84, http://dx.doi.org/10.1002/adfm.200901257.
[7] M.R. Koehler, V. Keppens, B.C. Sales, R. Jin, D. Mandrus, Elastic moduli of superhard rhenium diboride, J. Phys. D: Appl. Phys. 42 (2009) 095414–095418, http://dx.doi.org/10.1088/0022-3727/42/9/095414.
[8] H.-Y. Chung, M.B. Weinberger, J.B. Levine, A. Kavner, J.-M. Yang, S.H. Tolbert, R. B. Kaner, Synthesis of ultra-incompressible superhard rhenium diboride at ambient pressure, Science 316 (5823) (2007) 436–439, http://dx.doi.org/10.1126/science.1139322.
[9] J.B. Levine, S.L. Nguyen, H.I. Rasool, J.A. Wright, S.E. Brown, R.B. Kaner, Preparation and properties of metallic, superhard rhenium diboride crystals, J. Am. Chem. Soc. 130 (50) (2008) 16953–16958, http://dx.doi.org/10.1021/ja804989q.
[10] A. Latini, J.V. Rau, D. Ferro, R. Teghil, V.R. Albertini, S.M. Barinov, Superhard rhenium diboride films: preparation and characterization, Chem. Mater. 20 (13) (2008) 4507–4511, http://dx.doi.org/10.1021/cm800398s.
[11] F.M. Gao, L.H. Gao, Microscopic models of hardness, J. Superhard Mater. 32 (03) (2010) 148–166, http://dx.doi.org/10.3103/S1063457610030020.
[12] A.R. Oganov, A.O. Lyakov, Towards the theory of hardness of materials, J. Superhard Mater. 32 (03) (2010) 143–147.
[13] F. Gao, J. He, E. Wu, S. Liu, D. Yu, D. Li, S. Zhang, Y. Tian, Hardness of covalent crystals, Phys. Rev. Lett. 91 (1) (2003) 015502, http://dx.doi.org/10.1103/PhysRevLett.91.015502.
[14] F. Gao, Theoretical models of intrinsic hardness, Phys. Rev. B 73 (13) (2006) 132104, http://dx.doi.org/10.1103/PhysRevB.73.132104.
[15] A. Šimunek, J. Vackár, Hardness of covalent and ionic crystals: first-principle calculation, Phys. Rev. Lett. 96 (8) (2006) 085501, http://dx.doi.org/10.1103/PhysRevLett.96.085501.
[16] L. Fast, J. Wills, B. Johansson, O. Eriksson, Elastic constants of hexagonal transition metals: theory, Phys. Rev. B 51 (24) (1995) 431–438, http://dx.doi.org/10.1103/PhysRevB.51.17431.
[17] Y. Liang, B. Zhang, Mechanical and electrical properties of ReB_2, Phys. Rev. B 76. doi:10.1103/PhysRevB.76.132101.
[18] C. Wang, Q. Su, X. Song, B. Yu, First-principle study on the physical properties of ultra incompressible material ReB_2, Acta Metal. Sinica (English Letters) 22 (4) (2009) 284–290, http://dx.doi.org/10.1016/S1006-7191(08)60100-3.
[19] X. Zhu, D. Li, X. Cheng, Elasticity properties of the low-compressible material ReB_2, Solid State Commun. 147 (2008) 301–304, http://dx.doi.org/10.1016/j.ssc.2008.05.038.
[20] X. Hao, Z. Wu, Y. Xu, D. Zhou, X. Liu, J. Meng, Trends in elasticity and electronic structure of 5d transition metal diborides: first-principles calculations, J. Phys.: Condens. Matter 19 (19) (2007) 196212, http://dx.doi.org/10.1088/0953-8984/19/19/196212.
[21] S.Q. Wang, H.Q. Ye, Plane-wave pseudopotential study on mechanical and electronic properties for IV and III–V crystalline phases with zinc-blende structure, Phys. Rev. B 66 (2002) 235111, http://dx.doi.org/10.1103/PhysRevB.66.235111.
[22] M.-M. Zhong, X.-Y. Kuang, Z.-H. Wang, P. Shao, L.-P. Ding, X.-F. Huang, Phase stability, physical properties of rhenium diboride under high pressure and the effect of metallic bonding on its hardness, J. Alloy Compd. 581 (2013) 206–212, http://dx.doi.org/10.1016/j.jallcom.2013.07.068.
[23] M. Mazdziarz, T. Moscicki, Structural, mechanical, optical, thermodynamical and phonon properties of stable ReB_2 polymorphs from density functional calculations, J. Alloy Compd. 657 (2016) 878–888, http://dx.doi.org/10.1016/j.jallcom.2015.10.133.
[24] R. Dovesi, R. Orlando, B. Civalleri, C. Roetti, V.R. Saunders, C.M. Zicovich-Wilson, CRYSTAL: a program for the ab initio investigation of crystalline solids, Z. Kristallogr. 220 (5/6/2005) (2005) 571–573, http://dx.doi.org/10.1524/zkri.220.5.571.65065.
[25] C. Adamo, V. Barone, Toward reliable density functional methods without adjustable parameters: the PBE0 model, J. Chem. Phys. 110 (13) (1999) 6158–6170, http://dx.doi.org/10.1063/1.478522.
[26] D.C. Langreth, J.P. Perdew, Theory of nonuniform electronic systems. I. Analysis and a generalization that works, Phys. Rev. B 21 (12) (1980) 5469–5493, http://dx.doi.org/10.1103/PhysRevB.21.5469.
[27] D.C. Langreth, M.J. Mehl, Beyond the local-density approximation in calculations of ground-state electronic properties, Phys. Rev. B 28 (4) (1983) 1809–1834, http://dx.doi.org/10.1103/PhysRevB.28.1809.
[28] J.P. Perdew, K. Burke, M. Ernzerhorf, Generalized gradient approximation made simple, Phys. Rev. Lett. 77 (18) (1996) 3865–3868, http://dx.doi.org/10.1103/PhysRevLett.77.3865.
[29] J.P. Perdew, M. Ernzerhorf, K. Burke, Rationale for mixing exact exchange with density functional approximations, J. Chem. Phys. 105 (22) (1996) 9982–9985, http://dx.doi.org/10.1063/1.472933.
[30] H.J. Monkhorst, J.D. Pack, Special point of Brillouin-zone integration, Phys. Rev. B 13 (12) (1976) 5189–5192, http://dx.doi.org/10.1103/PhysRevB.13.5188.
[31] M.F. Peintinger, D.V. Oliveira, T. Bredow, Consistent gaussian basis sets of triple-zeta valence with polarization quality for solid calculations, J. Comput. Chem. 34 (6) (2013) 451–459, http://dx.doi.org/10.1002/jcc.23153.
[32] A. Erba, A. Mahmoud, R. Orlando, R. Dovesi, Elastic properties of six silicate garnet and members from accurate ab initio simulations, Phys. Chem. Miner. 41 (2) (2014) 151–160, http://dx.doi.org/10.1007/s00269-013-0630-4.
[33] W.F. Perger, J. Criswell, B. Civalleri, R. Dovesi, Ab-initio calculation of elastic constants of crystalline systems with the CRYSTAL code, Comput. Phys. Commun. 180 (2009) 1753–1759, http://dx.doi.org/10.1016/j.cpc.2009.04.022.
[34] C.A. Perottoni, A.S. Pereira, J.A.H. da Jornada, Periodic Hartree–Fock linear combination of crystalline orbitals calculation of the structure, equation of state and elastic properties of titanium diboride, J. Phys.: Condens. Matter 12 (2000) 7205–7222.
[35] J.W. Eaton, D. Bateman, S. Hauberg, GNU Octave Version 3.0.1 Manual: A High-Level Interactive Language for Numerical Computations, CreateSpace

Independent Publishing Platform. ISBN:1441413006, <http://www.gnu.org/software/octave/doc/interpreter>.
[36] A.M. Walker, J. Wookey, MSAT – a new toolkit for the analysis of elastic and seismic anisotropy, Comput. Geosci. 49 (2012) 81–90, http://dx.doi.org/10.1016/j.cageo.2012.05.031.
[37] C. Gatti, V.R. Saunders, C. Roetti, Crystal field effects on the topological properties of the electron density in molecular crystals: the case of urea, J. Chem. Phys. 101 (12) (1994) 10686–10696, http://dx.doi.org/10.1063/1.467882.
[38] C. Qi, Y. Jiang, Y. Liu, R. Zhou, Elastic and electronic properties of XB_2 (X=V, Nb, Ta, Cr, Mo, and W) with AlB_2 structure from first principles calculations, Ceram. Int. 40 (4) (2014) 5843–5851, http://dx.doi.org/10.1016/j.ceramint.2013.11.026.
[39] C. Stampfl, W. Mannstadt, R. Asahi, A.J. Freeman, Electronic structure and physical properties of early transition metal mononitrides: density-functional theory LDA, GGA, and screened-exchange LDA FLAPW calculations, Phys. Rev. B 63 (2001) 155106, http://dx.doi.org/10.1103/PhysRevB.63.155106.
[40] M.I. Aroyo, A. Kirov, C. Capillas, J.M. Perez-Mato, H. Wondratschek, Bilbao crystallographic server – II. Representations of crystallographic point groups and space groups, Acta Crystall. Sect. A 26 (2006) 115–118, http://dx.doi.org/10.1107/S0108767305040286.
[41] A. Kokalj, Computer graphics and graphical user interfaces as tools in simulations of matter at the atomic scale, Computat. Mater. Sci. 28 (2) (2003) 155–168, http://dx.doi.org/10.1016/S0927-0256(03)00104-6.
[42] W. Voigt, Lehrbuch Der Kristallphysik (mit Ausschluss Der Kristalloptik), Bibliotheca mathematica Teubneriana, B.G. Teubner, 1928. <https://books.google.com.co/books?id=3kSLnQEACAAJ>.
[43] S. Aydin, M. Simsek, First-principles calculations of MnB_2, TcB_2, and ReB_2 within the ReB_2-type structure, Phys. Rev. B 80 (2009) 134107, http://dx.doi.org/10.1103/PhysRevB.80.134107.
[44] P. Ravindran, L. Fast, P.A. Korzhavyi, B. Johansson, J. Wills, O. Eriksson, Density functional theory for calculation of elastic properties of orthorhombic crystals: application to $TiSi_2$, J. Appl. Phys. 84 (09) (1998) 4891–4904, http://dx.doi.org/10.1063/1.368733.
[45] J. Levine, J. Betts, J. Garrett, S. Guo, J. Eng, A. Migliori, R. Kaner, Full elastic tensor of a crystal of the superhard compound ReB_2, Acta Mater. 58 (5) (2010) 1530–1535, http://dx.doi.org/10.1016/j.actamat.2009.10.060.
[46] L.J. Walpole, The elastic shear moduli of a cubic crystal, J. Phys. D: Appl. Phys. 19 (1986) 457–462, http://dx.doi.org/10.1088/0022-3727/19/3/014.
[47] F. Peng, W. Peng, H. Fu, X. Yang, Elasticity and thermodynamic properties of RuB_2 under pressure, Physica B 404 (20) (2009) 3363–3367, http://dx.doi.org/10.1016/j.physb.2009.05.013.
[48] A. Reuss, Berechnung der fliessgrenze von mischkristallen auf grund der plastizitätsbedingung für einkristalle, Zeitschrift für Angewandte Mathematik und Mechanik 9 (1) (1929) 49–58, http://dx.doi.org/10.1002/zamm.19290090104.
[49] R. Hill, The elastic behaviour of a crystalline aggregate, Proc. Phys. Soc. A 65. doi:10.1088/0370-1298/65/5/307.
[50] S.I. Ranganathan, M. Ostoja-Starzewski, Universal elastic anisotropy index, Phys. Rev. Lett. 101 (2008) 055504, http://dx.doi.org/10.1103/PhysRevLett.101.055504.
[51] W. Zhou, H. Wu, T. Yildirim, Electronic, dynamical, and thermal properties of ultra-incompressible superhard rhenium diboride: a combined first-principles and neutron scattering study, Phys. Rev. B 76 (2007) 184113–184119, http://dx.doi.org/10.1103/PhysRevB.76.184113.
[52] S.C. Abrahams, F.S.L. Hsu, Debye temperatures and cohesive properties, J. Chem. Phys. 63 (3) (1975) 1162, http://dx.doi.org/10.1063/1.431443.
[53] C.F. Matta, R.J. Boyd, The Quantum Theory of Atoms in Molecules, Wiley-VCH, 2007.
[54] C. Gatti, Chemical bonding in crystals: new directions, Z. Kristallogr. 202 (2005) 399–457, http://dx.doi.org/10.1524/zkri.220.5.399.65073.
[55] X. Guo, L. Li, Z. Liu, D. Yu, J. He, R. Liu, B. Xu, Y. Tian, H.-T. Wang, Hardness of covalent compounds: roles of metallic component and d valence electrons, J. Appl. Phys. 104 (2) (2008) 023503, http://dx.doi.org/10.1063/1.2956594.